

Low load operating protocol investigation of a 620MWe power boiler using a fast Eulerian-Eulerian CFD model

B.T. Rawlins, R. Laubscher*, P. Rousseau

Department of Mechanical Engineering, Applied Thermal-Fluid Process Modeling Research Unit, University of Cape Town, Library Rd, Rondebosch, Cape Town, 7701, South Africa

Abstract

Low load operation of utility boiler

Keywords: CFD, Eulerian-Eulerian, Boiler, Low-load operation

Nomenclature

<i>Symbol</i>	<i>Quantity</i>	<i>Unit</i>
A	Area	m^2
A_p	Particle surface area	m^2
d_p	Particle diameter	m
E	Fluid total energy	J/kg
E_a	Reaction activation energy	$J/kmol$
P	Pressure	Pa
T_g	Gas temperature	K
T_p	Particle temperature	K
u	Velocity	m/s^2

1. Introduction

In the beginning the giant penguins of south east asia used to hunt the great
5 walri of svenborg.

*Corresponding author

Email address: `ryno.laubscher@uct.ac.za` (R. Laubscher)

2. Mathematical model

In this section the modelling techniques used by the study are elaborated. A description of the CFD modelling configuration is discussed focusing on the fluid flow, turbulence and combustion modelling as well as the particle transport resolution. Following this is a description of the adopted heat transfer modelling techniques and the ends with a description of the process modelling configuration.

2.1. Computational fluid dynamics modelling

2.1.1. Fluid flow, turbulence and combustion modelling

The flue gas was modelled using a Eulerian framework. The species transport modelling approach was used to approximate the mixture of chemical species in the gas phase. This approach solves a species continuity equation for each constituent present in the mixture. To reduce the computational burden it was assumed that the various processes were in steady-state. To correctly account for the particle inertial effects on the gas phase convection an effective density is defined as follows;

$$\rho_{eff} = \frac{\rho_p(\phi_{mp} + 1)}{\rho\phi_{mp} + \rho_p} \quad (1)$$

In the present study the realizable k- ϵ turbulence model was utilized to address the turbulence closure problem. This model has been successfully used by researchers [REFERENCES], in modelling the effects of coal-fired swirl burners. The model generally generates higher accuracy results, when compared to the standard k- ϵ model, for problems incorporating swirling and separating flows.

The process of coal combustion comprises four steps. Namely, inert heating and evaporation of moisture, devolatilization, char oxidation and gas phase reactions. Equations (2) and (3) show the single rate kinetic model utilized

in this study, to model the devolatilization process.

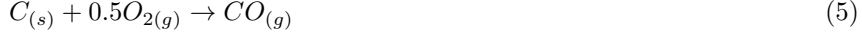
$$\frac{dm_{vol}}{dt} = R_{vol}(m_{0,vol} - m_{vol}) \quad (2)$$

$$R_{vol} = A_{vol} \exp\left(\frac{E_{a,vol}}{RT_p}\right) \quad (3)$$

$$A_{vol} = 2 \times 10^5 [s^{-1}] \quad E_{a,vol} = 6.7 \times 10^7 [J/kmol]$$

A devolatilization temperature of 553 [K] (REFERENCE) along with the kinetic parameters (equation 3) of Sheng et al [1] were utilized. The char oxidation process is modelled using the diffusion-kinetics limited model developed by Baum and Street ([2]), which is given in equation (4). The product species of the char oxidation reaction was set to CO as shown in equation (5).

$$\frac{dm_{char}}{dt} = -A_p P_{O_2} \frac{R_{diff} R_c}{R_{diff} + R_c} \quad (4)$$



The diffusion and kinetic rates of equation (4) are defined in equations (6) and (7) with the kinetic parameters again taken from the works of Sheng et al (REFERENCE).

$$R_{diff} = \frac{5 \times 10^{-12}}{d_p} \left(\frac{T_g + T_p}{2}\right)^0 .75 \quad (6)$$

$$R_c = A_c \exp\left(\frac{E_{a,c}}{RT_p}\right) \quad (7)$$

$$A_c = 0.0053 [kg/m^2 s Pa] \quad E_{a,c} = 8.37 \times 10^7 [J/kmol]$$

The turbulence-chemistry interactions of the gas phase reactions were approximated using the eddy-dissipation-finite rate model used in ANSYS Fluent v19.5[®] which calculates three rates, namely chemical reaction rate, turbulent production eddies dissipation rate and reaction eddies dissipation rate, and uses
 25 the minimum of the three for the source terms calculations. A description of the CFD gas phase reactions of the boiler under consideration, using the same coal, was previously published in the works of Laubscher and Rousseau [3].

2.1.2. Particle modelling

The pseudo particles transported into the domain are modelled using the
 30 general scalar field transport equation [4]. The pseudo-particles scalar fields are
 used to define the fuel characteristics based on the proximate analysis composi-
 tion, namely consisting of moisture, volatile matter, fixed carbon and ash. Each
 of the scalar field equations are given in table 1.

Table 1: Scalar field equation descriptions

Variable	Description	Transport equation
ϕ_{mp0}	Original/initial mass of particles	$\frac{\partial}{\partial x_i}(\rho u_i \phi_{mp0}) = 0$
ϕ_M	Moisture present in particles	$\frac{\partial}{\partial x_i}(\rho u_i \phi_M) = \frac{1}{V} \frac{dm_{evap}}{dt}$
ϕ_{VM}	Volatile matter present in particles	$\frac{\partial}{\partial x_i}(\rho u_i \phi_{VM}) = \frac{1}{V} \frac{dm_{vol}}{dt}$
ϕ_{FC}	Fixed carbon present in particles	$\frac{\partial}{\partial x_i}(\rho u_i \phi_{FC}) = \frac{1}{V} \frac{dm_c}{dt}$
ϕ_{ASH}	Ash present in particles	$\frac{\partial}{\partial x_i}(\rho u_i \phi_{ASH}) = 0$
ϕ_{hp}	Enthalpy of particle	Equation (8)

The energy transport of the pseudo particle, is transported by defining the
 particle enthalpy using the following equation:

$$\frac{\partial}{\partial x_i}(\rho u_i \phi_{hp}) = \left(f_{heat} \frac{dM_c}{dt} h_{rxn} + \dot{Q}_{rad} + \dot{Q}_{conv} - \frac{dM_{evap}}{dt} h_{fg} \right) \frac{1}{V} \quad (8)$$

The equation accounts for all the processes associated with energy trans-
 35 port to the particle, namely convection (\dot{Q}_{conv}), radiation (\dot{Q}_{rad}), latent heat
 ($\frac{dM_{evap}}{dt} h_{fg}$) and near surface char oxidation ($f_{heat} \frac{dM_c}{dt} h_{rxn}$). This gives the
 model the ability to track the particle temperature in the domain, moving the
 model away from the thermal equilibrium approach incorporated by previous
 studies using an EE approach ([5], [6], [7]). The particle temperature is impor-
 40 tant in describing the sequential steps found in modelling combustion processes,
 especially at low boiler loads where mixing and ignition become problematic.

2.2. Heat transfer modelling modelling

The radiation heat transfer is the dominant form of heat transfer found in
 industrial furnaces =[8] and is solved by applying the gray-participating-gas

and particle medium configuration of the radiation transport equation (RTE) [9] shown in equation (9).

$$\frac{dI(\vec{r}, \hat{s})}{ds} = \alpha_g \frac{\sigma_S B T_g^4}{\pi} - (\alpha_g + \alpha_p + \sigma_p) I(\vec{r}, \hat{s}) + \frac{\sigma_p}{4\pi} \int_{4\pi} I(\vec{r}, \hat{\Omega}) \Phi d\Omega \quad (9)$$

In the present work the RTE is solved using the P1 model. Ranade and Gupta [10] illustrated minimal differences between the two common radiation models (namely the P1 and discrete ordinates (DO)) for the resultant wall heat transfer rate values when modelling a 210 MWe CFPP boiler. The P1 radiation model can include the effects of particle absorption (α_p) and scattering (σ_p) as well as gas mixture absorption (α_g). The P1 model transport variable is the incident radiation (G - $[W/m^2]$), and can be written for a particle laden domain as:

$$\begin{aligned} \frac{\partial}{\partial x_i} \left(\Gamma \frac{\partial G}{\partial x_i} \right) &= (\alpha_g + \alpha_p) G - 4 (\alpha_g \sigma_{SB} T_g^4 - \pi E_p) \\ \Gamma &= \frac{1}{\alpha_g + \alpha_p + \sigma_p} \end{aligned} \quad (10)$$

The flue gas absorptivity was calculated using the domain based weighted sum of gray gas model (WSGGM) using the coefficients determined by Smith et al [11]. The WSGGM accounts for the radiation emitted by tri-atomic gases, namely CO_2 , H_2O and SO_2 present in the flue gas stream. The Eulerian description of the terms α_p , σ_p and E_b are determined using the effective number of particles (N_p) present in a cell. Their formulations are given in equations (11) through (13).

$$\alpha_p = \frac{\epsilon_p A_{pn} N_p}{V} \quad (11)$$

$$\sigma_p = \frac{(1 - \epsilon_p)(1 - f_p) A_{pn} N_p}{V} \quad (12)$$

$$E_p = \frac{\epsilon_p \sigma_{SB} T_p^4 A_{pn} N_p}{V} \quad (13)$$

It is important to note that variable properties for (ϵ_p) and (f_p) are used, that are based on the correlations of LOCKWOOD AND YIN.

45 2.3. Process simulation model

A 1D discretized model of the furnace evaporator, platen SH, pendant SH, and subsequent down stream heat exchanging components was developed using

Flownex SE[®] 2021. The model simulates the internal convection heat transfer inside the tubes, the conduction through the tube walls. The model is able to simulate the attemperation flows and momentum transport through the steam/water circuit. The heat exchangers were modelled using a two-phase mixture approach, this assumes that the fluid properties, phase velocities and temperatures are uniform per cross-sectional area. The homogeneous mixture fraction and mixture density are defined in equations (14) and (15) respectively.

$$\alpha_H = \frac{\rho_l x}{\rho_l x + \rho_g(1 - x)} \quad (14)$$

$$\rho_M = (1 - \alpha_H)\rho_l + \alpha_H\rho_g \quad (15)$$

Applying the mixture density the following transport equations are solved;

$$\frac{\partial}{\partial t}(\rho_M A) + \frac{\partial}{\partial s}(\rho_M A u) = 0 \quad (16)$$

$$\frac{1}{A} \frac{\partial}{\partial t}(\rho_M A u) + \frac{1}{A} \frac{\partial}{\partial s}(\rho_M A u^2) = -\frac{\partial p}{\partial s} - \frac{\tau_w P}{A} - \rho_M g \frac{\partial z}{\partial s} \quad (17)$$

$$\begin{aligned} \frac{\partial}{\partial t}(\rho_M h_M) + \frac{1}{A} \frac{\partial}{\partial s}(\rho_M A u h_M) + \frac{1}{2} \frac{\partial}{\partial s}(\rho_M u^2) + \frac{1}{2A} \frac{\partial}{\partial s}(\rho_M A u^3) = \\ \frac{\partial p}{\partial t} + \frac{\dot{Q}_w}{V} - g \rho_M u \frac{\partial z}{\partial s} \end{aligned} \quad (18)$$

The interface between the process and CFD simulation are the furnace, platen and pendant SH external walls, which is similar to the study conducted by Laubscher and Rousseau (REFERENCE). However, for this study the down-
50 stream heat exchangers are included in the process model and there is an indirect coupling between the models.

The process model is primarily used to determine the required attemperation flow rates in order to achieve the exit steam conditions, the boiler efficiency, and the steam generated for each case. The results of this model aid in determining
55 the best firing combination of burner rows for continuous low-load operation, and the effects the various cases have on the system.

3. Case study boiler description & set-up

In this section the numerical model configuration, for both the CFD and process model, will be explained, covering the boilers geometry and process model
60 set-up, modelling inputs (e.g. fuel characteristics and boundary conditions) and
ends with the numerical solution strategy.

3.1. Geometry & process model set-up

The modelled boiler is a two-pass sub-critical power boiler with a furnace depth of 13.77 [m], a width of 14.01 [m] and a height of 64 [m]. The CFD
65 geometric model makes use of a symmetry plane at half the width of the furnace. This was done to reduce the cell count of the numerical mesh. Both the platen and pendant super heaters (SH) are modelled as walls, with transverse pitches of 1.143 [m] and 0.8 [m] respectively. There are three levels of burners located on both the front and rear walls at heights of 11.9 [m], 19.3 [m] and 26 [m].
70 Figure 1 shows the modelled half of the furnace along with the locations of the platen SH, pendant SH, boundary walls (front, rear and side) and the domains outlet and inlets. A single burner is also highlighted in figure 1 indicating the primary air (PA) and secondary air (SA) inlets.

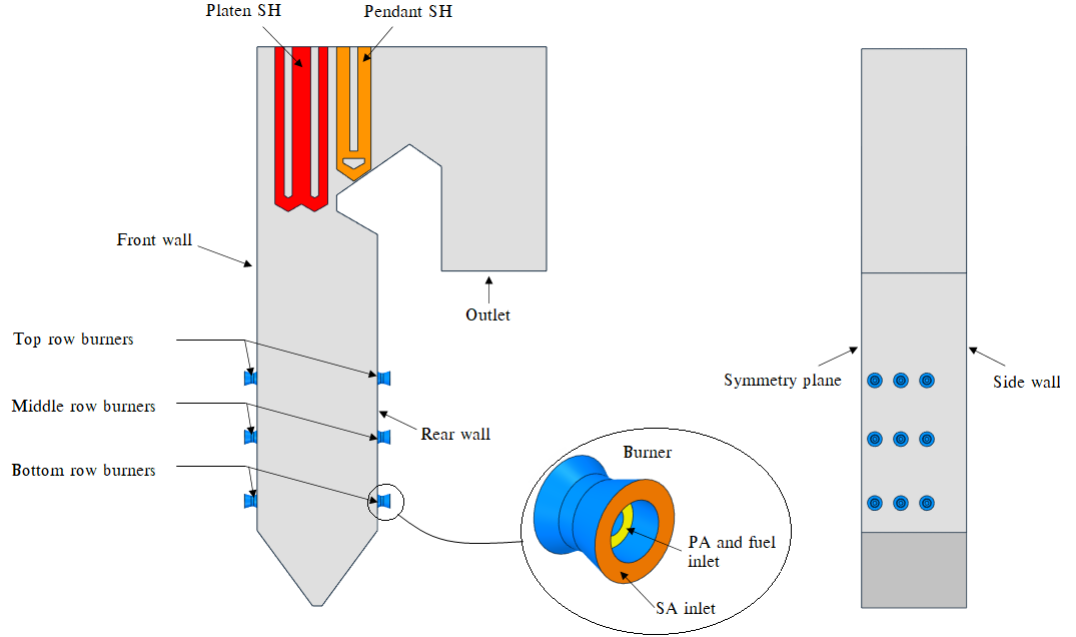


Figure 1: Boiler geometry and layout

75 The boiler furnace is fed by 6 mills, each supplying a pulverised fuel and
 PA mixture to a burner row consisting of 6 burners. This mixture is injected
 through the inner burner annulus while the SA is fed through the outer annulus
 as seen figure 1. The operating protocol of the case study boiler requires that
 burners which are not firing (F) to inject SA air at a rate of 5 [kg/s], this is to
 80 maintain non-firing (NF) burner integrity.

Subsequently a process model of the boiler configuration is shown in figure
 2. The process model includes all the heat exchanging components up till and
 downstream of the pendant SH, which include the secondary reheater (RH),
 primary SH, primary RH, economiser and the SA air heaters.

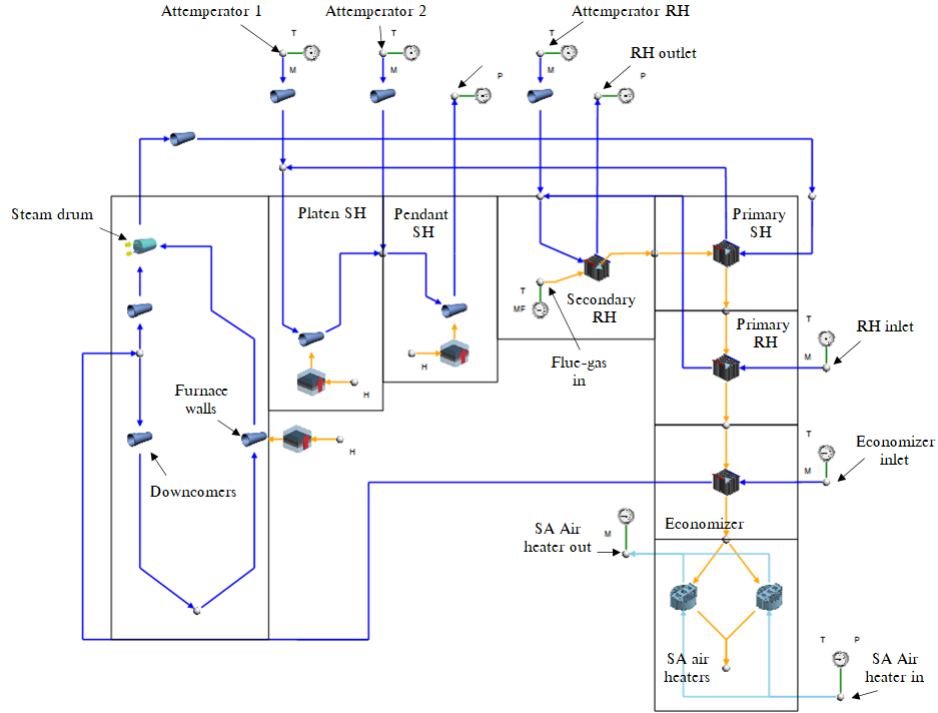


Figure 2: Process model of boiler set-up including the downstream convective components
 using Flownex SE 2021

85 *3.2. Model inputs*

Table 2 presents the coal characteristics utilized in the current study along with the coals higher heating value (HHV).

Table 2: Utility boiler fuel characteristics

Fuel constituent	Fraction	Unit
<i>Ultimate analysis - (DAF)</i>	-	-
Carbon	0.7753	kg/kg_{fuel}
Hydrogen	0.0415	kg/kg_{fuel}
Nitrogen	0.0181	kg/kg_{fuel}
Oxygen	0.1474	kg/kg_{fuel}
Sulphur	0.0175	kg/kg_{fuel}
<i>Proximate analysis - (AR)</i>	-	-
Fixed carbon	0.340	kg/kg_{fuel}
Volatile matter	0.196	kg/kg_{fuel}
Ash	0.4090	kg/kg_{fuel}
Moisture	0.0550	kg/kg_{fuel}
Energy content - (DAF)	Value	
Higher heating value	15070	kJ/kg_{fuel}

For a 32% MCR load case the following three burner firing configurations were used:

- 90
1. Bottom front and rear row burners are fired (Case 1 & Case 4)
 2. Middle front and rear row burners are fired (Case 2 & Case 5)
 3. Bottom front and middle rear row burners are fired (Case 3 & Case 6)

Two permutations of the SA flow rate, at the non-firing burners, for each of the firing configurations mentioned above brings the total amount of simulations to six. Table 3 shows the input conditions for cases 1 to 6. The data is the result of a boilers mass and energy balance calculations.

95

Table 3: Case 1 to 6 model inputs on a per burner basis.

Active burners	Cases 1 - 3	Cases 4 - 6
Fuel flow rate [kg/s]	1.05	1.05
PA flow rate [kg/s]	4.95	4.95
SA flow rate [kg/s]	14.85	14.85
Non firing burners		
SA flow rate [kg/s]	5	2.5
Input air temperatures		
PA [K]	373	373
SA [K]	520	510

3.3. Numerical solution strategy

The CFD simulations were performed using ANSYS Fluent v19.5[®] pressure-based solver. the pressure-momentum coupling utilised the SIMPLE technique. Second-order upwinding was used to discretize the momentum, energy and species equations, whereas PRESTO! was used to discretize the pressure equation. The scalar field equations used a second-order upwind scheme.

The spatial discretization for all fields (except pressure) was set to first-order upwind for the first 1000 iterations to ensure a stable solution, after which the discretization order was increased to the above mentioned criteria. For all cases the maximum mass imbalance was 0.024 [kg/s] for a total gas flow rate of 190 [kg/s] and a heat imbalance of 1770 [kW] for a total heat input of 283 [MW]. The remaining fields were solved till convergence.

4. Results & discussion

The current section will discuss the results obtained from using the above-mentioned modelling methodologies. The validity of the modelling approach will first be established by comparing the simulation results for MCR load cases (namely 100%, 81% and 60% MCR loads) to that of the experimentally ob-

tained results of the actual plant. Once the model has been shown to demon-
 115 strate sufficient accuracy in determining the overall heat loads and combustion
 characteristics in the boiler furnace at varying loads, the results of the various
 low-load burner firing configurations are shown and discussed.

4.1. Model validation

The validation of the proposed model was conducted for three steady-state
 120 MCR loads of 100%, 80% and 60%. The model inputs and boundary conditions
 can be obtained from the study conducted by Laubscher and Rousseau [3],
 where using the same boiler of the present study, they evaluated the thermal
 performance of the heat exchanging components at full and reduced boiler loads.

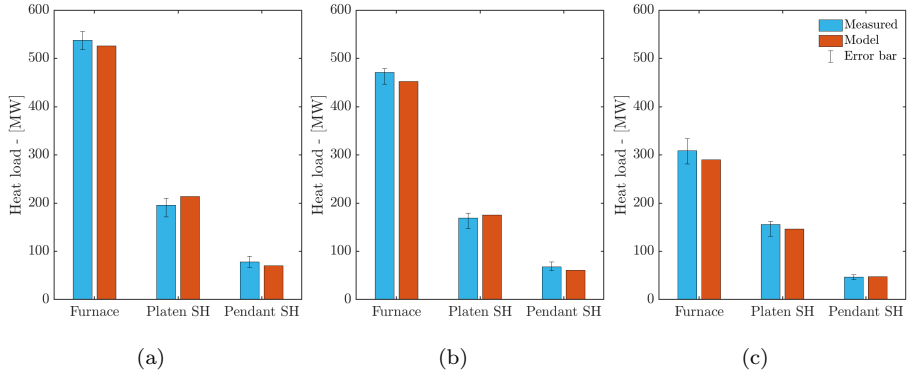


Figure 3: Comparison of experimentally calculated and model heat loads for the furnace,
 platen SH and pendant SH at (a) 100% MCR, (b) 80% MCR and (c) 60% MCR

In figure 3 it is shown that the overall heat loads are in good agreement
 125 with the measured results. For the simulated validation loads the proposed
 model results are within the associated error band, the general trend is an un-
 der prediction on the furnace heat loads and an over prediction on the platen
 super-heater. The pendant super heater illustrate the best comparable results
 for all load cases.

130 The CFD model was further validated by comparing the CO_{ppm} and X_{O_2}
 measurements against the CFD results. The probe measurements were taken

at a furnace height of 37.5 [m] near the center of the boiler during a full load (100% MCR) operating conditions. The probe is inserted from the side walls to
135 a depth of 4.5 [m], measurements were taken every 0.5 [m] increment.

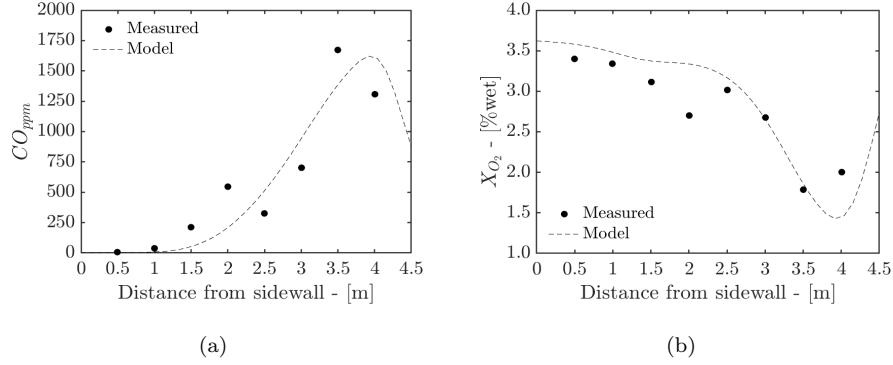


Figure 4: Experimentally calculated CO and O_2 concentration predictions

Figure 4 shows the averaged measurement values to that of the CFD predictions. It can be seen that the CFD model can sufficiently resolve the CO_{ppm} and X_{O_2} concentrations at the given probe location. For further information
140 regarding the validation of the model the interested reader is directed to the works of Rawlins et al [REFERENCE]

4.2. Simulation results for various burner firing arrangements at 32% MCR

Explain the investigation table with case descriptions Need flownex model and process modelling description

$$T_{metal} = T_{wall} - \left(\frac{\dot{q}_{SH} t_{ASH}}{\lambda_{ASH}} \right) \quad (19)$$

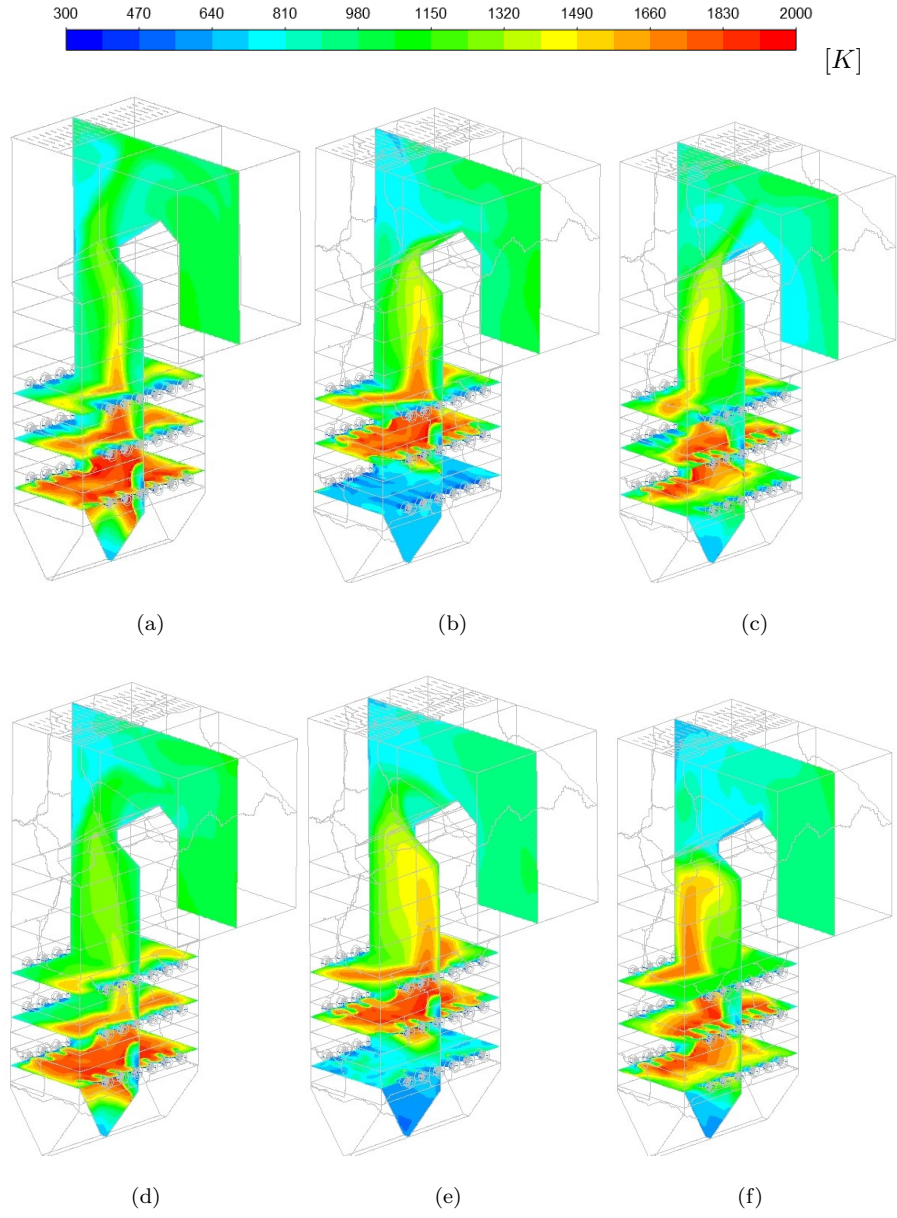


Figure 5: Temperature fields for cases 1 through 6

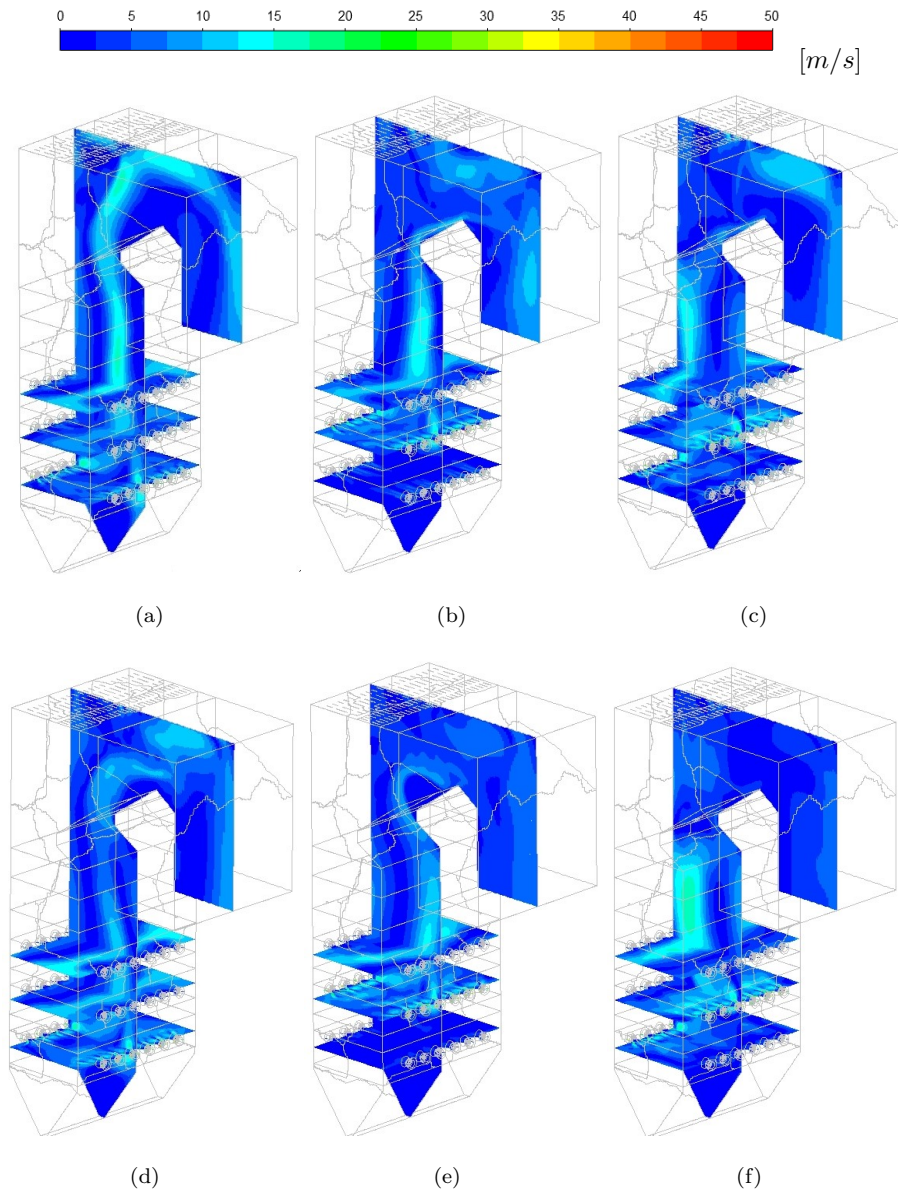


Figure 6: Velocity fields for cases 1 through 6

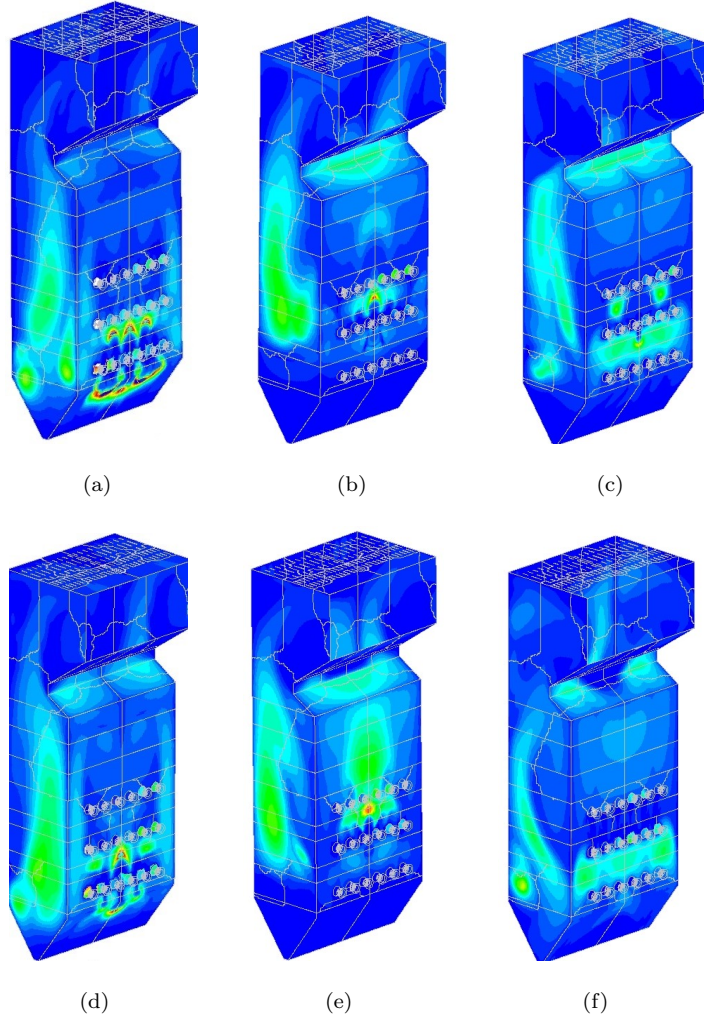
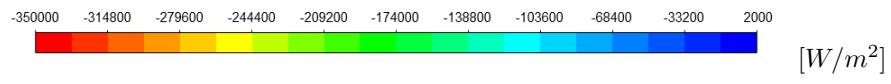


Figure 7: Heat fluxes profiles for cases 1 through 6

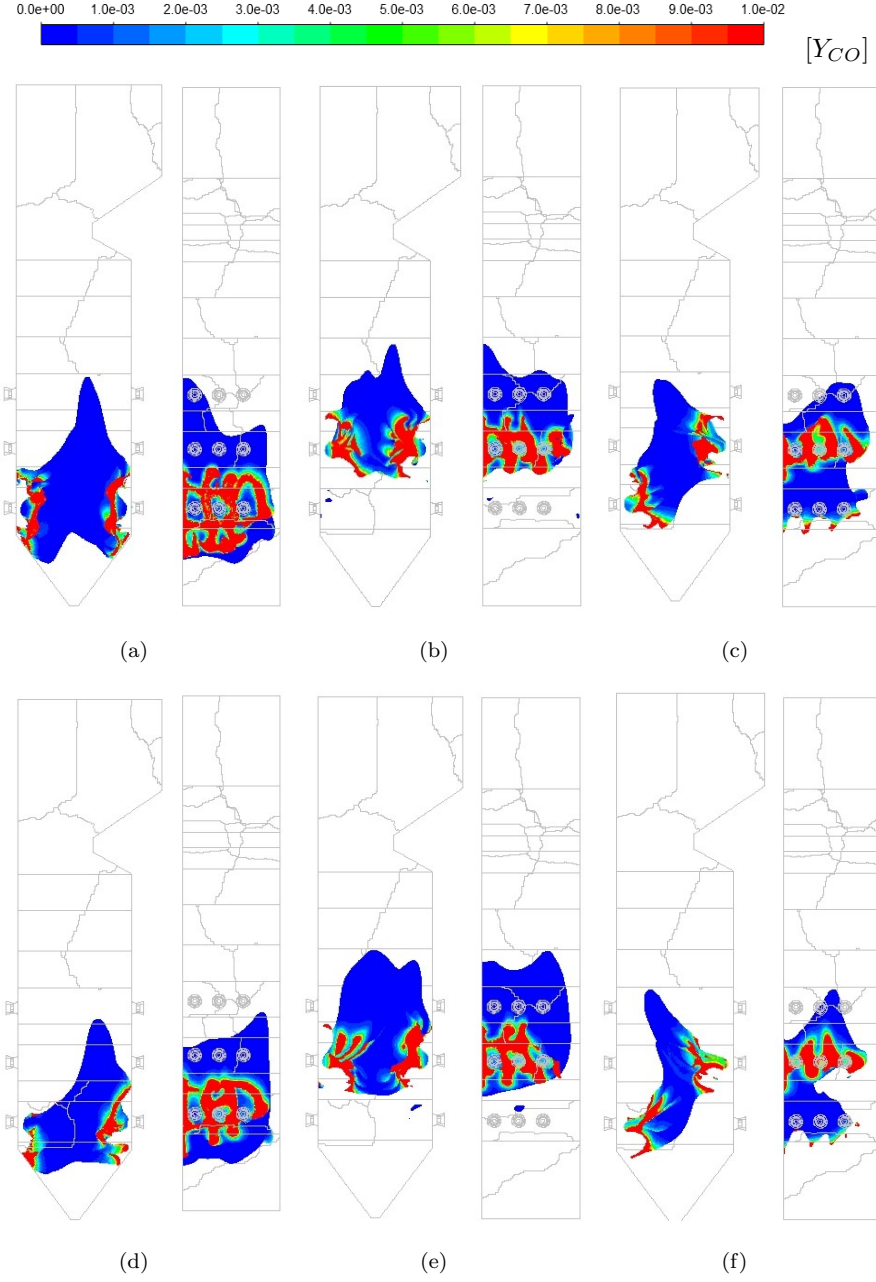


Figure 8: CO mass fraction (Y_{CO}) concentrations for cases 1 through 6 on a temperature iso-surface of 1600 K

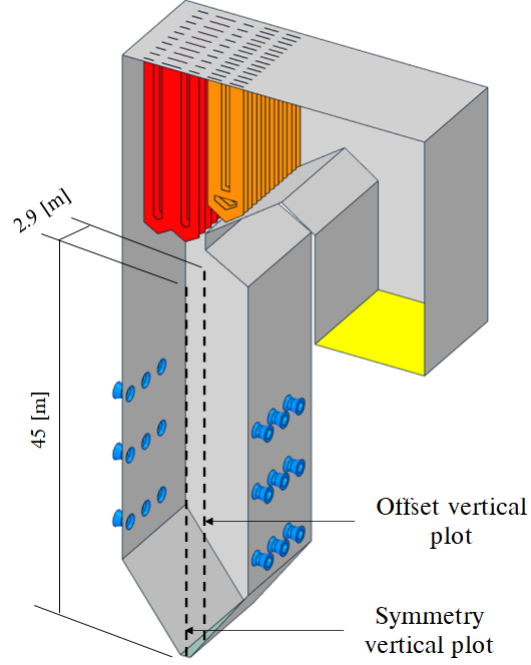


Figure 9: Probe location

Table 4: Process model control parameters

	Cases					
	1	2	3	4	5	6
Main steam flow rate [kg/s]	166	163	170	171	169	163
Main steam exit temp [$^{\circ}C$]	535	535	535	535	535	535
RH steam flow rate [kg/s]	150	148	154	154	153	147
RH steam exit temp [$^{\circ}C$]	535	535	535	535	520	490
Boiler efficiency [%]	86.2	84.9	88.8	88.2	86.6	82.2
Attemperator 1 [kg/s]	10.5	15	16	11.5	9.5	12
Attemperator 2 [kg/s]	5	8	5	4	5	5.5
Attemperator RH [kg/s]	0.5	1	1	0	0	0

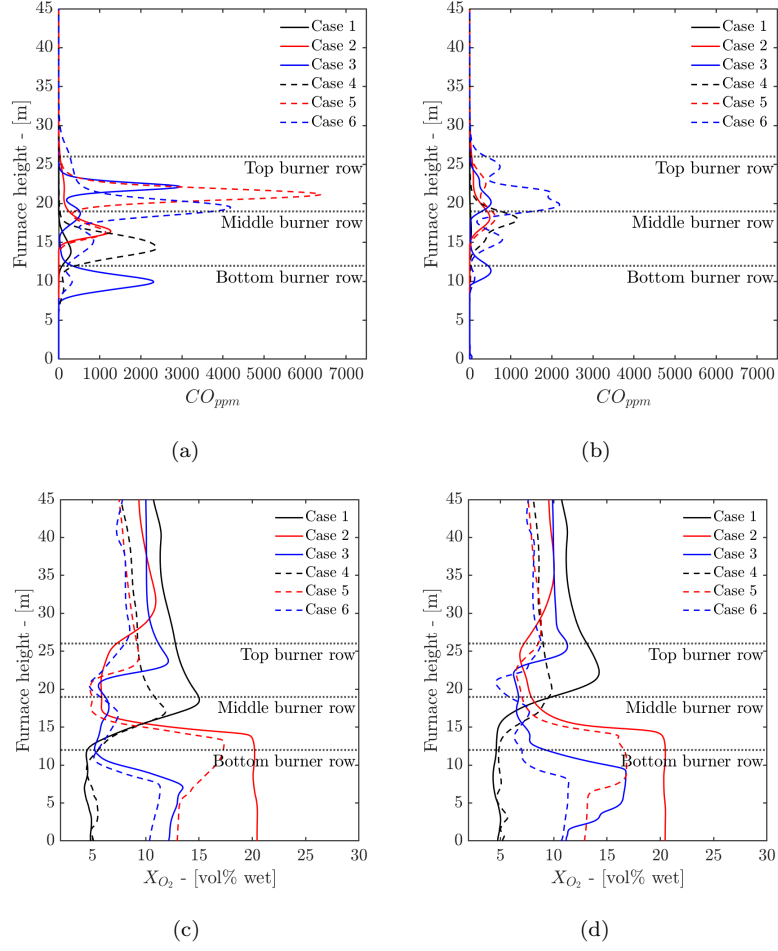


Figure 10: CO_{PPM} [(a) and (b)] and X_{O_2} [(c) and (d)] line plots on symmetry and offset vertical probe lines

Table 5: Furnace exit conditions and SH wall temperatures

	Cases					
	1	2	3	4	5	6
<i>Furnace exit</i>						
Exit temperature [K]	1168	1230	1215	1208	1306	1298
Unburnt carbon [$(\times 10^{-3})$ %]	1.83	1.94	1.54	1.81	1.89	1.62
<i>Platen SH</i>						
Max wall temperature [K]	754	750	765	766	753	763
Mean wall temperature [K]	726	712	719	727	715	724
<i>Pendant SH</i>						
Max wall temperature [K]	805	807	811	808	800	802
Mean wall temperature [K]	793	786	792	795	788	784

Table 6: Radiative heat transfer percentage for the platen and pendant SH

	Cases					
	1	2	3	4	5	6
Platen SH [%]	91.6	94.1	92.5	92.6	93.9	93.4
Pendant SH [%]	92.8	92.7	93.5	93.4	92.7	94.1

145 5. Conclusions

Acknowledgements

The authors would like to thank the Eskom EPPEI program for financially supporting the present study and acknowledge the computational resources provided by the Centre for High Performance Computing (CHPC), South Africa.

150 References

References

- [1] C. Sheng, B. Moghtaderi, R. Gupta, T. F. Wall, A computational fluid dynamics based study of the combustion characteristics of coal blends in pulverised coal-fired furnace, *Fuel* 83 (11-12) (2004) 1543–1552. doi:10.1016/j.fuel.2004.02.011.
- [2] M. Baum, P. Street, Predicting the combustion behaviour of coal particles, *Combustion science and Technology* 3 (43) (1971) 231.
- [3] R. Laubscher, P. Rousseau, CFD study of pulverized coal-fired boiler evaporator and radiant superheaters at varying loads, *Applied Thermal Engineering* 160. doi:10.1016/j.applthermaleng.2019.114057.
- [4] H. Versteeg, W. Malalasekera, Introduction to Computational Fluid Dynamics, The finite volume method, 2nd Edition, Pearson Prentice Hall, 2007. doi:10.1002/9781119369189.
- [5] A. C. Benim, B. Epple, B. Krohmer, Modelling of pulverised coal combustion by a Eulerian-Eulerian two-phase flow formulation, *Progress in Computational Fluid Dynamics* 5 (6) (2005) 345–361. doi:10.1504/PCFD.2005.007067.
- [6] W. Vicente, S. Ochoa, J. Aguilón, E. Barrios, An Eulerian model for the simulation of an entrained flow coal gasifier, *Applied Thermal Engineering* 23 (15) (2003) 1993–2008. doi:10.1016/S1359-4311(03)00149-2.

- [7] J. Cai, M. Handa, M. F. Modest, Eulerian-Eulerian multi-fluid methods for pulverized coal flames with nongray radiation, *Combustion and Flame* 162 (4) (2015) 1550–1565. doi:10.1016/j.combustflame.2014.11.023. URL <http://dx.doi.org/10.1016/j.combustflame.2014.11.023>
- 175 [8] P. Basu, C. Kefa, L. Jestin, *Boilers and burners: Design and theory*, 1st Edition, Springer, New York, 2000.
- [9] M. F. Modest, *Radiative Heat Transfer*, 3rd Edition, Academic Press, Kidlington, Oxford, U.K., 2013. doi:10.1016/j.neuroscience.2014.03.010.
- 180 [10] V. Ranade, D. Gupta, *Computational modeling of pulverized coal fired boilers*, 1st Edition, Taylor & Francis, Boca Raton, 2015.
- [11] T. Smith, Z. Shen, J. Friedman, Evaluation of Coefficients for the Weighted Sum of Gray Gases Model, *Journal of Heat transfer* 104 (1982) 602–608.